Check for updates

Study on mechanism of elemene reversing tumor multidrug resistance based on luminescence pharmacokinetics in tumor cells *in vitro* and *in vivo*

Liying Chen, [iD] †[a] Zhi Chen,†*[ab] Shuang Zheng,[a] Luhui Fan,[a] Lixin Zhu,[ac] Jiandong Yu,[a] Chaoyuan Tang,[a] Qi Liu[d] and Yang Xiong*[a]

While elemene (ELE) can reverse tumor multidrug resistance (MDR), the mechanisms for ELE reversing MDR remain unclear. Numerous studies have suggested that the efflux functionality of ATP-binding cassette (ABC) transporters, not their quantity, is more relevant to tumor MDR. However, no appropriate methods exist for real-time detection of the intracellular drug efflux caused by ABC transporters *in vitro*, especially *in vivo*, which hinders the examination of MDR reversal mechanisms. This study directly investigates the correlation between efflux functionality of ABC transporters and MDR reversal *via* ELE, using D-luciferin potassium salt (D-luc) as the chemotherapeutic substitute to study the intracellular drug efflux. Here, a luciferase reporter assay system combined with bioluminescence imaging confirmed that the efflux of D-luc from MCF-7/DOX^{Fluc} cells *in vitro* and *in vivo* was significantly reduced by ELE and when combined with Doxorubicin (DOX), ELE showed a synergistically anti-tumor effect *in vitro* and *in vivo*. Additionally, the luminescence pharmacokinetics of D-luc in MCF-7/DOX^{Fluc} cells and pharmacodynamics of the combined ELE and DOX *in vivo* showed a great correlation, implying that D-luc might be used as a probe to study ABC transporters-mediated efflux in order to explore mechanisms of traditional Chinese medicines reversing MDR.

1. Introduction

Cancer is regarded as one of the most serious diseases, and chemotherapy remains a key treatment method for different stages and many types of cancer. However, the efficiency of clinical therapy remains poor and unsatisfactory.[1,2] One of the most prominent obstacles to universally effective chemotherapy remains tumor multidrug resistance (MDR), which is the intrinsic or acquired resistance of tumor cells to a wide range of drugs with diverse structures and functions.[3,4]

Numerous studies have validated ATP-binding cassette (ABC) transporters-such as ABCB1 (also called P-glycoprotein), ABCC1 (also called MRP1), and ABCG2 (also called BCRP)-as the main players for MDR to distinct anti-tumor drugs.[5–9] Chemical MDR reversal agents-such as verapamil,[10] cyclosporin A,[11] and tamoxifen[12] have limited application because of their high toxicities, side effects, and unobvious reversal effect when combined with chemotherapies.[13] Comparatively, some

traditional Chinese medicines (TCMs) have shown a significant MDR reversal effect with fewer side effects.[14–16] In our former studies, we found that several TCMs-such as elemene (ELE), a noncytotoxic broad-spectrum anti-tumor drug extracted from *Curcuma zedoaria Roscoe* have great reversal effect in MDR cells. However, these TCMs do not always reduce the expression of MDR-related ABC transporters.[17] Interestingly, some TCMs decrease the expression of ABC transporters in tumor cells *in vitro* but have less or no effect *in vivo* or *vice versa*. That means there may be no direct correlation between the quantity of ABC transporters *in vitro* and *in vivo*. Do these TCMs directly affect the functionality of ABC transporters and then changing the drug efflux from tumor cells? Is there a direct correlation between the functionality of ABC transporters *in vitro* and *in vivo*? Regretfully, the mechanisms of these TCMs reversing MDR remain unclear today. Thus, identifying a method to examine the functionality of ABC transporters *in vitro*, especially *in vivo*, is of particular importance to reversing MDR.

In this paper, D-luciferin potassium salt (D-luc), a specific substrate of ABC transporters, served as the substitute for chemotherapeutics in studying the effect of intracellular drug efflux treated by ELE. As both D-luc and most small molecule chemotherapeutics are substrates of ABC transporters, their uptake into or efflux from tumor cells should be very similar.[18] A luciferase reporter assay system combined with biolumines-cence imaging (BLI) technology was applied to examine the

[a]Department of Pharmaceutical Science, College of Pharmaceutical Science, Zhejiang Chinese Medical University, Hangzhou 311400, Zhejiang, China

[b]The First People's Hospital of Jiande, Jiande 311600, Zhejiang, China

[c]Zhejiang Institute for Food and Drug Control, Hangzhou 310004, Zhejiang, China

[d]Department of Dermatology, Johns Hopkins University School of Medicine, Baltimore, MD 21231, USA

† These authors made equal contributions to this work.

uptake or efflux fluorescence kinetics of D-luc in tumor cells in real time. When D-luc enters tumor cells, it is catalyzed by luciferases based on energy-dependent reactions in form of visible lights emitting photons under the specific wavelengths, which can be quantitatively monitored in real-time by BLI.[19] A BLI-based assay also allows for noninvasive real-time monitoring of biological processes in many disease models, such as cancers.[20] Additionally, the assay's high signal-to-noise and low background allow for accurately examining cells that stably express a small amount of luciferase, requiring as little as 10^{-19} mol of luciferase.[21] Furthermore, the factors that determine the BLI intensity involve the oxygen and substrate concentration, the presence of magnesium ions, and the expression level of luciferase.[22] Several papers have confirmed that ABC transporters impact readout intensity of BLI in intact living cells by greater efflux of substrates such as D-luc, which is a vital aspect of several potential confusing factors affecting BLI values.[23] Since the luciferase reporter is only constructed in tumor cells,[24,25] the readout should only show the D-luc in tumor cells, even *in vivo*. Combining pharmacokinetics (PK) modeling with BLI, a more exact set of PK parameters would be obtained, which has been confirmed in the former study.[26] Thus, the fluorescence PK of D-luc *in vitro* and *in vivo* should be highly related and could be used as an effective probe to reflect drug efflux from tumor cells.

Ultimately, this research aimed to study the mechanisms of ELE reversing breast cancer MDR *via* evaluating the functionality of ABC transporters based on the PK of D-luc *in vitro* and *in vivo* in MCF/DOX^{Fluc} cells. Then, ELE combined with DOX was injected into on MCF/DOX^{Fluc} cells and tumor-bearing nude mice to study the effects. Finally, the following relationships were analyzed by Pearson correlation analysis: (1) between the PK of D-luc *in vitro* and *in vivo*, (2) between the PK of D-luc *in vitro* and the PD of the combined ELE and DOX *in vitro*, and (3) between the PK of D-luc *in vivo* and the PD of the combined ELE and DOX *in vivo*.

2. Materials and methods

2.1 Materials

D-luc was provided by Thermo Fisher Scientific (USA). ELE (purity ≥ 98%) was obtained from Dalian Holley Kingkong Pharmaceutical Company (Dalian, China). Doxorubicin (DOX) was obtained from Hisun Pharmaceutical Company (Hangzhou, China). The BCA protein quantitation kit and RIPA lysis buffer were provided by Beyotime Biotechnology (Shanghai, China). Verapamil and Ko143 were obtained from Apexbio (Houston, USA). Fetal bovine serum (FBS) was provided by Bioind (Israel). Phosphate-buffered saline (PBS) was purchased from Northend Company (Hangzhou, China). Penicillin/ streptomycin (P/S), Dulbecco's Modified Eagle's Medium (DMEM), and 0.25% trypsin–EDTA were obtained from Gibco (USA). All cell culture supplies (culture flask, Petri dish, well plates) were purchased from Corning Incorporated (USA). Matrigel was provided by BD Biosciences (USA). Thiazolyl blue tetrazolium bromide (MTT) was obtained from Sigma-Aldrich

(USA). All chemicals for the experiment were analytical reagent grade.

2.2 Cell line and experimental animals

The MCF-7/DOX cells (DOX-resistant human breast cancer cells) were kindly presented by Sichuan University (Sichuan, China) and routinely grew in DMEM medium containing 1% P/S and 10% FBS and incubated at 5% CO_2 and 37 °C. The MCF-7/ DOX^{Fluc} cell line, which stably expresses the firefly luciferase reporter gene, was constructed by lentivirus infection in our former studies.[26]

The nude mice (aged 4–5 weeks, female, BALB/c) were provided by Slake Laboratory Animal Company (Shanghai, China) and bred by Zhejiang Chinese Medical University Laboratory Animal Research Center (Hangzhou, China). Then, to establish the xenograft models, 6×10^7 of MCF-7/DOX^{Fluc} cells and Matrigel at a ratio of 1 : 1 suspended in 200 μL of PBS were inoculated subcutaneously into the right flank of mice. Briefly, all animal experiments were performed in accordance with the National Institutes of Health Guidelines on Laboratory Research and approved by the Animal Care Committee at Zhejiang Chinese Medical University.

2.3 *In vitro* cytotoxicity studies

The cytotoxicity of MCF-7/DOX^{Fluc} cells and the effect of ELE reversing MDR were evaluated using a standard MTT assay. MCF-7/DOX^{Fluc} cells were seeded in 96-well plates at the density of 7×10^3 cells per well for 24 h. Subsequently, cells were incubated with different samples, which were either exposed to DOX alone or in combination with ELE at a ratio of 1 : 3, to check the cell viability and proliferation. After the treating period and washing the cells with PBS, fresh medium containing MTT (0.5 mg mL^{-1}) was added to each well, and the plates were maintained at 37 °C for another 4 h. Briefly, the MTT solution was completely replaced by 150 μL of DMSO to dissolve the formed formazan salt. The absorbance of each well was detected at 570 nm by a Bio-Tek microplate reader. Each concentration was tested for at least 3 wells, and the data were performed as mean ± SD. Then, the half maximal inhibitory concentration (IC$_{50}$) values were presented by GraphPad Prism V6.01 software. Each sample was repeated in triplicate. Cell viability (%) was presented using the following equation: $[(OD_{sample} - OD_{blank\ control})/(OD_{positive\ control} - OD_{blank\ control})] \times 100$. Then, the combination index (CI) analysis of combination ELE and DOX was examined by CompuSyn software.

2.4 *In vivo* anti-tumor efficacy and systemic toxicity

Xenografts of human breast cancer were used as described in Section 2.2. MCF/DOX^{Fluc} tumor-bearing nude mice were used to examine tumor inhibition efficacy of ELE at different concentrations in combination with DOX. The mice were divided randomly into 6 groups ($n = 6$) and treated with saline, ELE (10 mg kg^{-1}, 25 mg kg^{-1}, i.p.), DOX (5 mg kg^{-1}, i.v.), and DOX (5 mg kg^{-1}, i.v.) combined with ELE (10 mg kg^{-1}, 25 mg kg^{-1}, i.p., given 1 h before DOX treatment). The DOX was given twice a week for 4 weeks, and ELE was given every other day.

Additionally, body weights were weighed and recorded twice a week. The tumor volume was recorded twice a week and then calculated using the following equation: volume (V) = length (L) × width^2 (W^2) × 1/2. At the end of treatment, the major organs and tumors were collected for hematoxylin and eosin (H&E) staining to evaluate specific toxicity.

2.5 *In vitro* fluorescence kinetics of D-luc in MCF-7/DOX^{Fluc} cells analysis

To investigate the effect of ELE on the functionality of ABC transporters *in vitro*, the efflux kinetic of D-luc from MCF-7/DOX^{Fluc} cells was noninvasively monitored, and the change of luminescent intensity was quantitatively measured by BLI in real time. MCF-7/DOX^{Fluc} cells were seeded in 96-well solid black plate at the density of 7×10^3 cells per well. After cells attached for 24 h, Ko143 (inhibitors of ABCG$_2$, 5 μmol L^{-1}) and verapamil (inhibitors of ABCB1, 10 μmol L^{-1}) alone were used as control or treated with ELE at varying concentrations (5 μg mL^{-1} and 20 μg mL^{-1}), and incubated for different time (24 h, 48 h, and 72 h). Then D-luc was put into each well and immediately kinetically imaged using an *in vivo* imaging system (IVIS) (Xenogen, USA). The luminescent intensity values of intracellular photon signals were caught every 5 min for a total of 115 min to acquire the efflux kinetics of D-luc. Relative BLI (BLI$_{rel}$) meant the photon signal intensity of each group normalized *via* total protein content to eliminate the confounding influence of increasing cell populations of photon signaling intensity. The data was calculated to obtain BLI$_{rel}$ *versus* time curves. *Via* the non-compartment model method, the dynamic parameters (AUC, MRT) of D-fluorescein potassium in cells were calculated.

2.6 *In vivo* fluorescence kinetics of D-luc in MCF-7/DOX^{Fluc} cells analysis

Different concentrations of D-luc directly affects the luminescent intensity. To detect optimal luminescent intensity, the appropriate concentration is crucial for the trials. The mice were intraperitoneally injected with different concentrations of D-luc (50 mg kg^{-1}, 75 mg kg^{-1}, and 100 mg kg^{-1}). To obtain the efflux kinetics of D-luc *in vivo*, the BLI signals of each time point were quantitatively recorded within 180 min. The photon signaling intensity of each time point was normalized by the volume of tumors in each treatment group and considered as BLI$_{rel}$. Subsequently, the acceptable concentration of D-luc could be applied in the following studies.

To acquire the efflux kinetics of D-luc under the intervention of ELE at different concentrations (10 mg kg^{-1}, 25 mg kg^{-1}), the BLI signals were taken at every time point for 0–115 min by using the IVIS kinetic imaging system after treating with ELE at a series of time points (7 d, 14 d, and 21 d). The BLI signal was also normalized as above. *Via* the non-compartment model method, the dynamic parameters-area under the curve (AUC) and mean residence time (MRT) of D-luc were calculated.

2.7 *In vivo* and *in vitro* correlation analysis

The correlation between the PK of D-luc and the PD of combined efficiency of DOX with ELE was explored to evaluate fluorescence efflux dynamics using D-luc, which served as a probe. The PK of D-luc used dynamic parameters (AUC, MRT) as the main indicators which respectively represented the intracellular accumulation and efflux rate of D-luc. The viability rate of MCF-7/DOX^{Fluc} cells and the tumor inhibition rate, respectively, were used as the
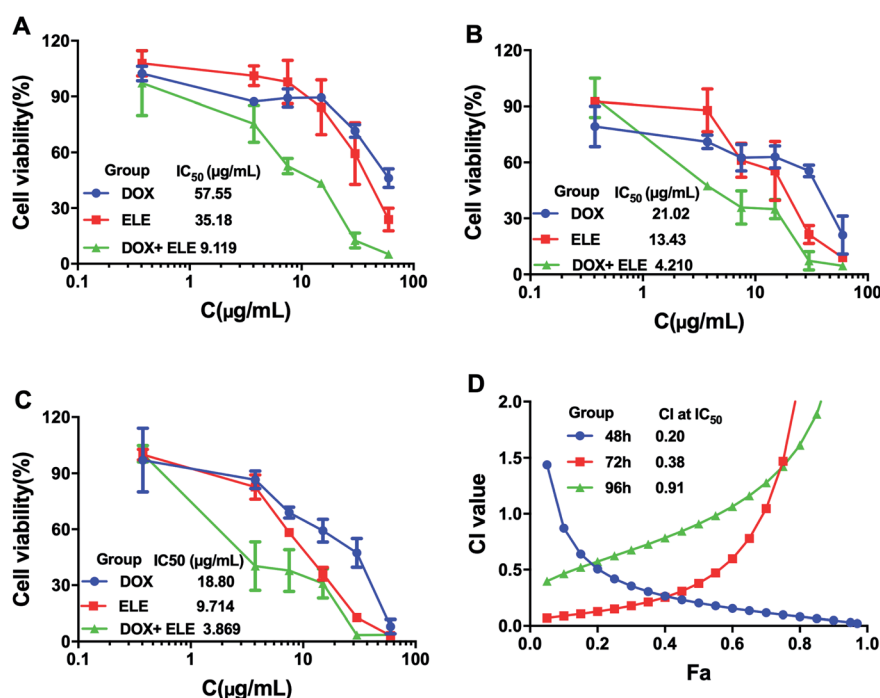

Fig. 1 Cell viability of MCF-7/DOX^{Fluc}. MCF-7/DOX^{Fluc} cells were treated with ELE and DOX alone or in combination for (A) 48 h, (B) 72 h, and (C) 96 h. (D) Synergistic index curve of combination group treating on MCF-7/DOX^{Fluc} cells for 48 h, 72 h, and 96 h. Data are mean ± SD ($n = 3$).

main indexes for the PD of the combined ELE and DOX *in vitro* and *in vivo*. Three following relationships were analyzed using Pearson correlation analysis: (1) between the PK of D-luc *in vitro* and *in vivo*, (2) between the PK of D-luc *in vitro* and the PD of the combined ELE and DOX *in vitro*, and (3) between the PK of D-luc *in vivo* and the PD of the combined ELE and DOX *in vivo*.

2.8 Statistical analysis

Data was shown as mean $\pm$ SD ($n > 3$). Combining SPSS 20.0 software, the statistical analysis of data was determined using

the Student *t*-test. The statistically significant difference was defined as *$P < 0.05$, **$P < 0.01$, and ***$P < 0.001$.

3. Results

3.1 ELE inhibited the viability of MCF-7/DOX^{Fluc} cells *in vitro*

The effects on the viability of MCF-7/DOX^{Fluc} cells after treating with ELE and DOX alone or in combination at different time points were evaluated (Fig. 1A–C). The results showed that the ELE, DOX, and ELE combined with DOX inhibited the viability
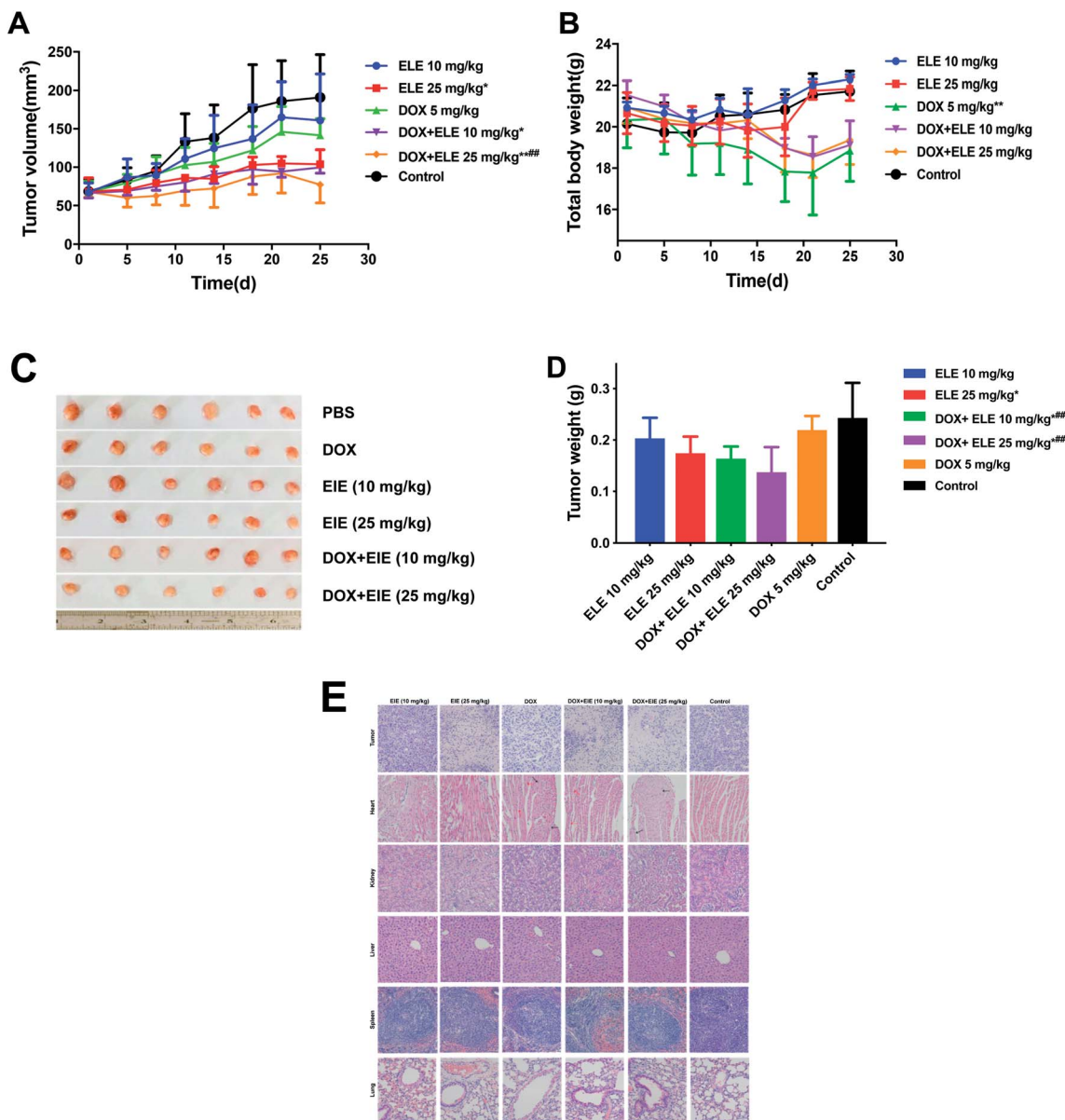

Fig. 2 Tumor inhibition effects and systemic toxicity of DOX, ELE, and DOX in combination with ELE on MCF-7/DOX^{Fluc} tumor-bearing nude mice. (A) The nude mice were treated with DOX (5 mg mL^{-1}, i.v.) and ELE (10 mg mL^{-1} and 25 mg mL^{-1}, i.p.) or the combination of both drugs. The tumor volumes were measured twice a week. *$P < 0.05$; **$P < 0.01$ *vs.* control; $^{\#}P < 0.05$, $^{\#\#}P < 0.01$ *vs.* DOX group. (B) Effect of different drugs on body weight of tumor-bearing nude mice. The body weights were measured twice a week. *$P < 0.05$; **$P < 0.01$ *vs.* control. (C) Visual observations of tumor size in per treatment group at the end time point. (D) Tumor mean (with SD) weights were measured 24 h after the last injection. *$P < 0.05$ *vs.* control group; $^{\#\#}P < 0.01$ *vs.* the DOX group. (E) H&E staining of major organs and tumor tissues from tumor-bearing nude mice that received last treatment (20×). Data are mean $\pm$ SD ($n = 6$).
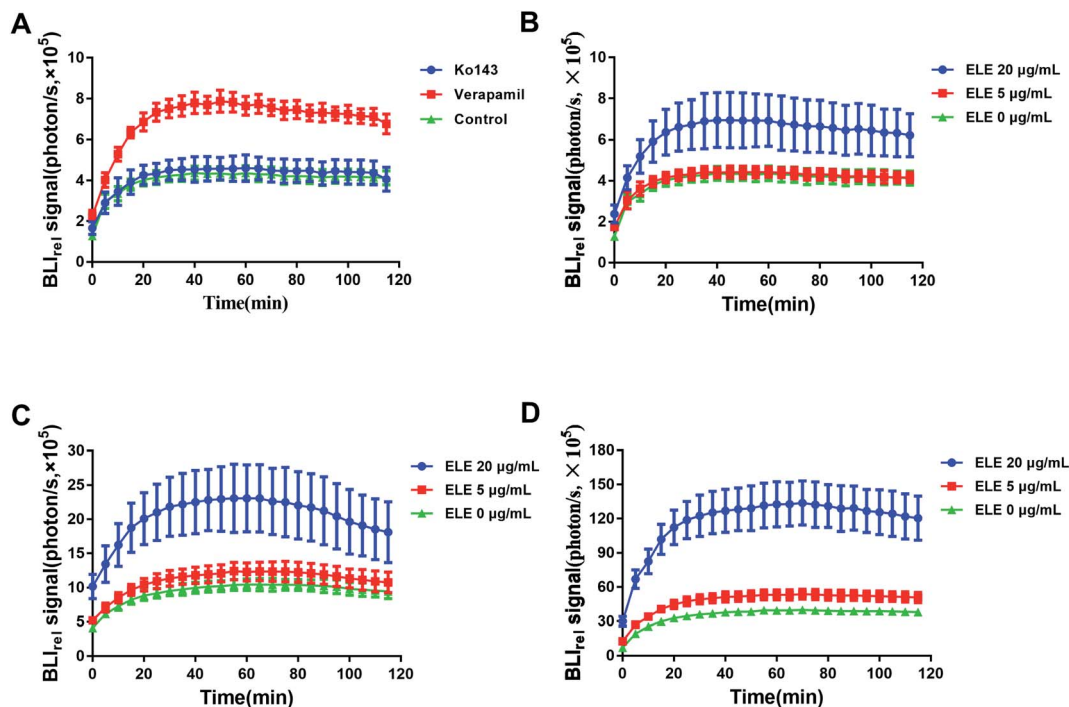
Fig. 3 BLI_{rel} signal photon–time curve of MCF-7/DOX^{Fluc} at different treatments *in vitro*. (A) Treated with verapamil and Ko143 for 24 h ($x \pm$ SD, $n = 6$). Treated with ELE at different concentrations for (B) 24 h, (C) 48 h, and (D) 72 h. Data are mean $\pm$ SD ($n = 6$).

Table 1 Pharmacokinetic parameters of BLI_{rel} data ($n = 6$, mean $\pm$ SD)[a]

Parameters	Verapamil ($\mu g\ mL^{-1}$)	Ko143 ($\mu g\ mL^{-1}$)	Control
AUC ($\times 10^7$)	6.7 $\pm$ 1.5**	5.0 $\pm$ 0.6	4.5 $\pm$ 0.4
MRT	625.3 $\pm$ 177.8***	359.4 $\pm$ 147.3***	1211.0 $\pm$ 270.6

[a] **$P < 0.01$, ***$P < 0.001$ *vs.* control.

of MCF-7/DOX^{Fluc} cells, and ELE was revealed to enhance the cytotoxicity of DOX on MCF-7/DOX^{Fluc} cells. More narrowly, the IC_{50} values of DOX at different time points (48 h, 72 h, and 96 h) were 57.55 $\mu g\ mL^{-1}$, 21.02 $\mu g\ mL^{-1}$, and 18.80 $\mu g\ mL^{-1}$, respectively, demonstrating that the increased cytotoxicity of DOX on MCF-7/DOX^{Fluc} cells was time-dependent. The CIs of ELE and DOX were calculated by CompuSyn software, and the result indicated that ELE and DOX had a synergistical effect to reduce the cytotoxicity of DOX to MCF-7/DOX^{Fluc} cells (Fig. 1D).

3.2 ELE enhanced the inhibition of the MCF-7/DOX^{Fluc} breast cancer xenogeneic model *in vivo*

The tumor inhibition efficiency is shown in Fig. 2A–D. Comparing with the PBS group, the group treated with ELE (10 mg kg^{-1}, i.p.) or DOX (5 mg kg^{-1}, i.v.) alone exhibited mild reductions in the growth rate of tumors, while the combined DOX and ELE produced significant tumor growth inhibition effects ($p < 0.05$). The decrement of tumor weight (Fig. 2D) in mice treated by DOX combined with ELE was significantly lower than in the DOX group. Besides, H&E-stained tumor sections revealed that the internal tumor tissues were almost completely necrotic in the combined group (Fig. 2E). Additionally, the H&E staining showed a significant decrease in renal toxicities and slightly decreased cardiotoxicity in the combined group. This result demonstrated that ELE enhanced the anti-tumor efficacy and decrease the toxicity of DOX.

Table 2 Pharmacokinetic parameters of BLI_{rel} data *in vitro* ($n = 6$, mean $\pm$ SD)[a]

Concentration ($\mu g\ mL^{-1}$)	AUC_{luc} ($\times 10^7$)			MRT_{luc}		
	24 h	48 h	72 h	24 h	48 h	72 h
0	4.5 $\pm$ 0.3	10.5 $\pm$ 0.8	39.4 $\pm$ 1.9	1030.8 $\pm$ 466.2	305.8 $\pm$ 50.5	971.8 $\pm$ 163.9
5	4.6 $\pm$ 0.3	12.41 $\pm$ 1.2**	53.4 $\pm$ 4.1**	789.8 $\pm$ 93.6	263.3 $\pm$ 48.2	909.5 $\pm$ 108.3
20	7.1 $\pm$ 1.2***	23.0 $\pm$ 4.4***	131.8 $\pm$ 17.6***	469.4 $\pm$ 198.7*	186.2 $\pm$ 46.3**	554.9 $\pm$ 241.7*

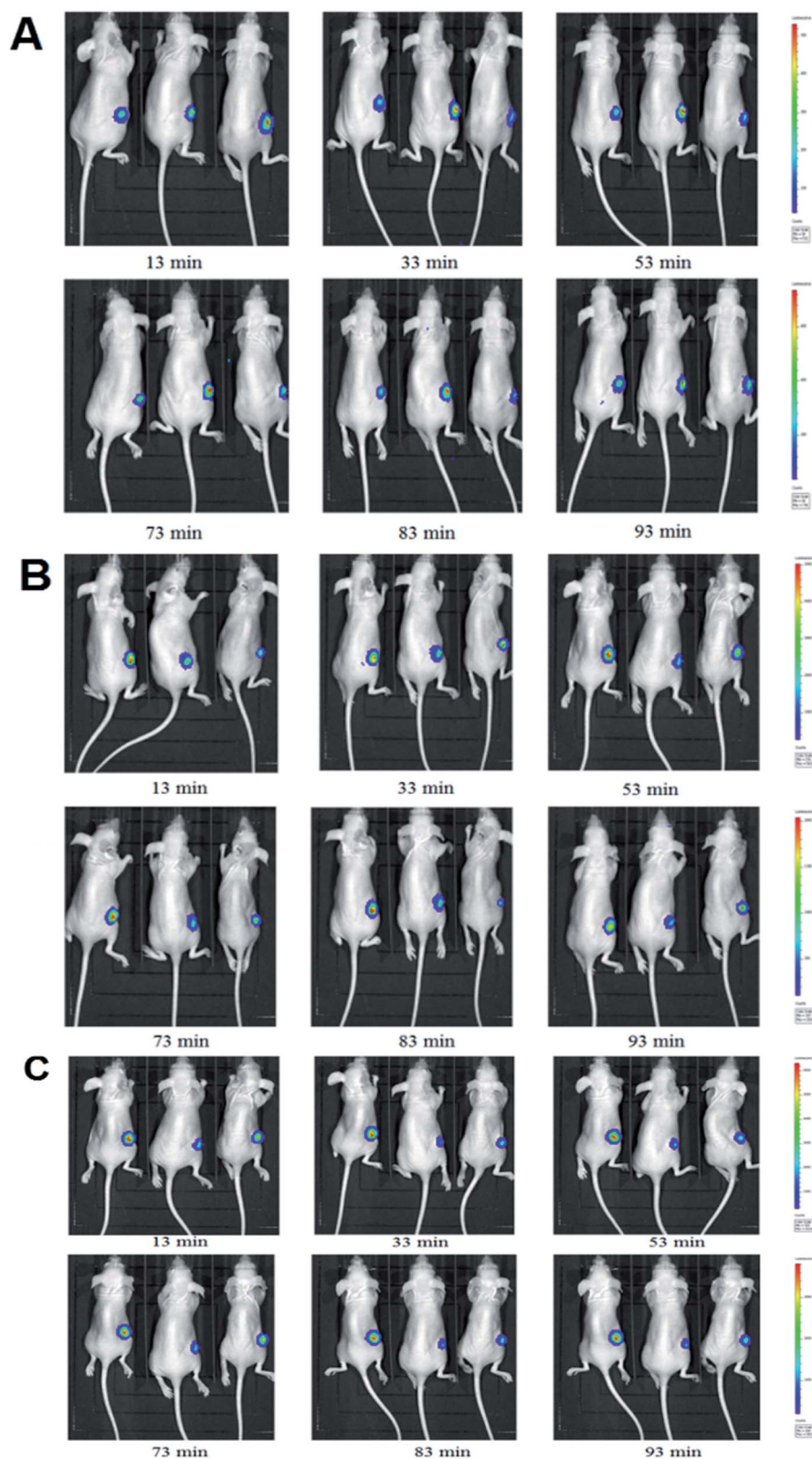[a] *$P < 0.05$, **$P < 0.01$, ***$P < 0.001$ *vs.* control.

Fig. 4 BLI of MCF-7/DOX^{Fluc} tumor-bearing nude mice at different time points within 115 min after intraperitoneal injected D-luc with a dose of 100 mg kg^{-1} ($n = 3$). (A) PBS group (i.p., QD). (B) The low ELE concentration group (ELE 10 mg kg^{-1}, i.p., QD). (C) The high ELE concentration group (ELE 25 mg kg^{-1}, i.p., QD).
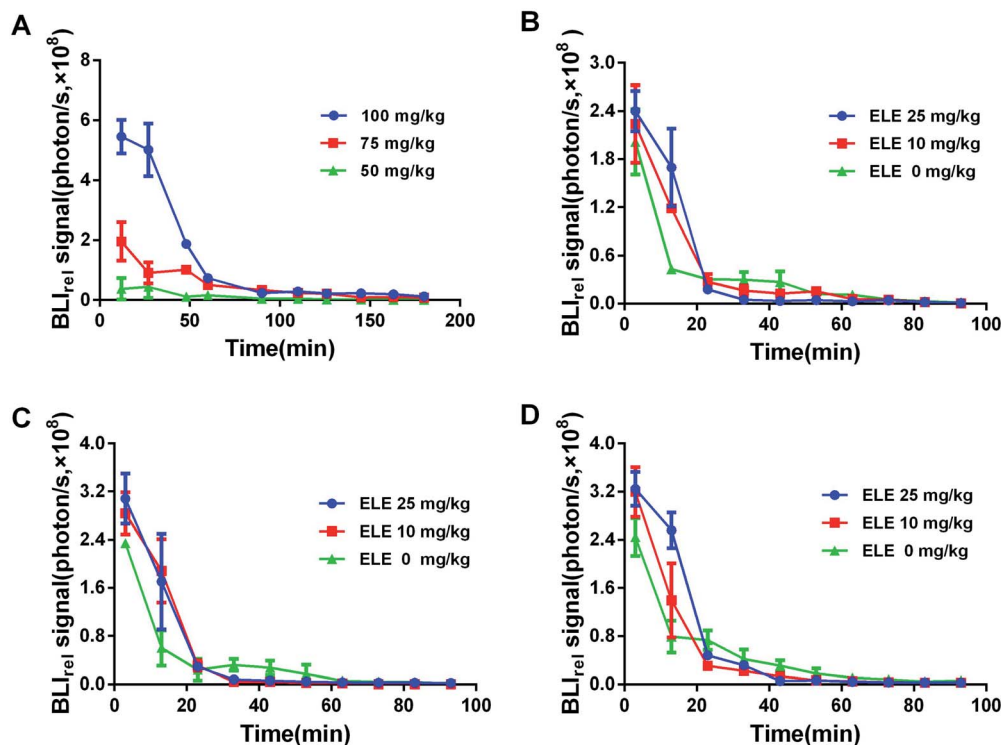
Fig. 5 BLI_{rel} signal photon–time curve of MCF-7/DOX^{Fluc} tumor-bearing nude mice at different treatments. (A) Bioluminescence response of D-luc at different concentrations. Treated with different ELE concentrations for (B) 7 d, (C) 14 d, and (D) 21 d. Data are mean $\pm$ SD ($n = 3$). The data are normalized to the 115 min time point.

3.3 ELE inhibited the functionality of ABC transporters in MCF-7/DOX^{Fluc} cells *in vitro*

The efflux kinetic of D-luc in MCF-7/DOX^{Fluc} cells was non-invasively monitored. The luminescent intensity change was measured using IVIS after treating MCF-7/DOX^{Fluc} cells with the ABCG2/BCRP inhibitor Ko143 and the ABCB1 inhibitor verapamil (Fig. 3A), or with the ELE with varying concentrations for 24 h, 48 h, and 72 h (Fig. 3B–D). The result showed that ELE might weaken the elimination of intracellular D-luc, which caused the same trend as ABC transporter inhibitors Ko143 or verapamil. Compared with the control, the ABCB1 inhibitor verapamil (Table 1), and ELE at 20 µg mL^{-1} (Table 2) significantly increased the AUC, Ko143, verapamil and ELE suppressed MRT significantly ($P < 0.05$). These findings meant that Ko143 and verapamil could, to some extent, inhibit the functionality of ABC transporters, and verified that ELE could obviously increase the intracellular accumulation of D-luc to reduce its efflux by affecting the functionality of ABC transporters.

3.4 ELE inhibited the functionality of ABC transporters in MCF-7/DOX^{Fluc} cells *in vivo*

The luminescent intensity in tumor cells significantly enhanced with increasing concentration of D-luc (Fig. 5A). Since the concentration of 75 mg kg^{-1} D-luc was unsaturated while detected, it was chosen for the subsequent studies of BLI signal detection. BLI signals of the MCF-7/DOX^{Fluc} cells could be detected after i.p. injection of D-luc (Fig. 4). Tumor-bearing nude mice were i.p.-injected with 100 µL of D-luc after pretreatment of ELE (10 mg kg^{-1} and 25 mg kg^{-1}, respectively) for different time points (7 d, 14 d, and 21 d) and then used for BLI. As shown in Fig. 5B–D, the BLI_{rel} was gradually increased over time. Additionally, the parameters were calculated according to the non-compartmental model. The AUC of ELE-treated groups was

Table 3 Pharmacokinetic parameters of BLI_{rel} data *in vivo* ($n = 6$, mean $\pm$ SD)^a

Concentration (mg kg^{-1})	AUC$_{luc}$ ($\times 10^9$)			MRT$_{luc}$		
	7 d	14 d	21 d	7 d	14 d	21 d
0	3.1 ± 0.4	3.6 ± 0.1	4.5 ± 0.2	20.6 ± 0.7	17.9 ± 0.7	25.2 ± 5.1
10	3.6 ± 0.1	4.9 ± 0.6	5.4 ± 0.1	15.9 ± 1.6	14.5 ± 3.5	15.6 ± 0.3
25	3.7 ± 0.5	5.1 ± 0.8	5.7 ± 0.6	$11.2 \pm 0.7^{**}$	$13.3 \pm 0.6^{*}$	13.9 ± 0.2

^{a} $^*P < 0.05$, $^{**}P < 0.01$ *vs.* control.

Table 4 Correlation of AUC (PK) *in vitro* and *in vivo* after ELE treatment

Group	Pearson coefficient	P
ELE 5 mg kg^{-1}	0.755	0.041
ELE 20 mg kg^{-1}	0.881	0.02

Table 5 Correlation between cell viability (PD) and AUC (PK) *in vitro* after ELE treatment

Group	Pearson coefficient	P
ELE 5 μg mL^{-1}	−0.971	0.001
ELE 20 μg mL^{-1}	−0.753	0.042

higher than that of control group after 7 d, 14 d, and 21 d, whereas the MRT of ELE-treated groups was lower than for the control group (Table 3). This finding meant that, with the time-growth of ELE treatments, the intracellular efflux rate of D-luc in MCF/DOX^{Fluc} cells *in vivo* was reduced, while the intracellular accumulation was increased and concentration-dependent.

3.5 A correlation existed between the PK of D-luc in MCF-7/DOX^{Fluc} cells *in vitro* and *in vivo*

After treating MCF-7/DOX^{Fluc} cells with ELE with varying concentrations (5 μg mL^{-1}, and 20 μg mL^{-1}) at different time points (24 h, 48 h, and 72 h), the AUC of D-luc in MCF-7/DOX^{Fluc} cells *in vivo* and *in vitro* was analyzed using Pearson correlation analysis. The results indicated that the AUC *in vitro* was positively correlated with the AUC *in vivo* in all ELE groups, and the Pearson correlation coefficient values were more than 0.7 ($P < 0.05$) (Table 4).

3.6 A correlation existed between the PK of D-luc in MCF-7/DOX^{Fluc} cells and PD of the combined ELE and DOX *in vitro*

The viability of MCF-7/DOX^{Fluc} cells after being treated with ELE (5 μg mL^{-1}, and 20 μg mL^{-1}) and the AUC in MCF-7/DOX^{Fluc} cells at different time points (24 h, 48 h, and 72 h) were analyzed using Pearson correlation analysis. The AUC was negatively correlated with the cell viability in all ELE groups, which is shown in Table 5. The absolute Pearson correlation coefficient values for ELE groups (5 μg mL^{-1} and 20 μg mL^{-1}) were 0.971 ($P < 0.01$) and 0.753 ($P < 0.05$), respectively.

3.7 A correlation existed between the PK of D-luc in MCF-7/DOX^{Fluc} cells and PD of the combined ELE and DOX *in vivo*

The tumor inhibition on MCF/DOX^{Fluc} tumor-bearing nude mice was obtained by combined ELE (5 mg kg^{-1} and 10 mg

Table 6 Correlation between tumor inhibition rate (PD) and AUC (PK) *in vivo* after ELE treatment

Group	Pearson coefficient	P
ELE 5 mg kg^{-1}	0.965	0.002
ELE 20 mg kg^{-1}	0.890	0.017

kg^{-1}) with DOX for 7 d, 14 d, and 21 d. The correlation between the AUC of D-luc *in vivo* and tumor inhibition was analyzed using Pearson correlation analysis. The results, listed in Table 6, showed a strong correlation between AUC and PD *in vivo*. The Pearson correlation coefficient values were 0.965 ($P < 0.01$) and 0.89 ($P < 0.05$), respectively.

4. Discussions

MDR reversing in cancer is a challenging task because it can be caused by many complex mechanisms, such as increased efflux of drugs, disordered cell apoptosis pathway, impaired DNA replication and repair capacity, altered drug target, and so on.[27–32] Following a general number of studies, it has been widely recognized that the primary reason of MDR is the increased efflux of anti-tumor drugs *via* overexpression or abnormal functionality of membrane-embedded ABC transporters.[33–35] Studies have shown that the drug efflux are not necessarily linked to the quantity while the functionality of ABC transporters. Now fluorescent dye rhodamine 123 (P-gp substrate) was already applied to determine the functional activity of ABC transporters in MDR cells quantitatively,[35] but it failed to dynamically detect the luminescence pharmacokinetics in cell in real time, which must be subsequently analyzed by flow cytometry or high-performance liquid chromatography to determine the cellular content of rhodamine 123. Furthermore, it cannot evaluate the functionality of ABC transporters in live animals *in vivo*.

In our study, by combining firefly luciferase with BLI technology, the MDR reversing mechanisms of ELE were validated by directly exploring the functionality of ABC transporters through the real time altering of the cellular efflux of D-luc (substitute for chemotherapeutics) *in vitro*, especially *in vivo*. BLI detects the generated light by luciferase-catalyzed reactions of substrates which is especially suitable for observing biological processes, such as *in vitro* and *in vivo* when monitoring kinetic profiles of carriers or drugs.[36] Several studies found a correlation between BLI dynamics and D-luc uptake and efflux mechanisms.[37,38] In this paper, our findings revealed that the reversing MDR mechanism on human breast cancer of ELE was to inhibit the drug efflux by weakening the functionality of ABC transporters. Since D-luc efflux from the cell could be detected both *in vitro* and *in vivo* in real time, a good correlation between the efflux PK of D-luc *in vitro* and *in vivo* were also established. This finding offers a possible molecular mechanism to highlight the cellular uptake kinetics of D-luc so that it might serve as an effective probe for reflecting the drug efflux in tumor cells. It also suggests that firefly luciferase reporter assay system combined with BLI is useful for studying ABC transporters-mediated efflux by TCMs which are of higher efficacy and lower toxicity.

5. Conclusions

At present, many studies have found that the combination of traditional Chinese medicine and chemotherapeutic drugs showed a good reversal MDR effect. However, the reversal MDR

mechanism is not very clear and it is difficult to establish an effective correlation between the reversal effect of TCM *in vitro* and *in vivo*. In this paper, we used BLI technology combined with luciferase reporter gene technology to achieve a non-injury, real-time, dynamic and quantitative characterization of ABC transporter substrate D-luc effluxing from live tumor cells *in vitro* and *in vivo*. This method could be used to evaluate the functionality of ABC transporters affected by MDR reversal agent and make it possible to establish a positive correlation between the reversal effect *in vivo* and *in vitro*.

Conflicts of interest

There are no conflicts to declare.

Acknowledgements

References

1 R. L. Siegel, K. D. Miller and A. Jemal, Cancer statistics, 2018, *Ca-Cancer J. Clin.*, 2018, **60**(5), 7–30.

2 W. Chen, R. Zheng, P. D. Baade, S. Zhang, H. Zeng, F. Bray, *et al.*, Cancer statistics in China, 2015, *Ca-Cancer J. Clin.*, 2016, **66**(2), 115–132.

3 W. Li, H. Zhang, Y. G. Assaraf, K. Zhao, X. Xu, J. Xie, *et al.*, Overcoming ABC transporter-mediated multidrug resistance: molecular mechanisms and novel therapeutic drug strategies, *Drug Resist. Updates*, 2016, **27**, 14–29.

4 Y. Zhang, Z. Wu, H. Yu, H. Wang, G. Liu, S. Wang, *et al.*, Chinese Herbal Medicine Wenxia Changfu Formula Reverses Cell Adhesion-Mediated Drug Resistance *via* the Integrin β1-PI3K-AKT Pathway in Lung Cancer, *J. Cancer*, 2019, **10**(2), 293–304.

5 S. Ranjbar, R. Khonkarn, A. Moreno, H. Baubichon-Cortay, R. Miri, M. Khoshneviszadeh, *et al.*, 5-Oxo-hexahydroquinoline derivatives as modulators of P-gp, MRP1 and BCRP transporters to overcome multidrug resistance in cancer cells, *Toxicol. Appl. Pharmacol.*, 2019, **362**, 136–149.

6 R. W. Robey, K. M. Pluchino, M. D. Hall, A. T. Fojo, S. E. Bates and M. M. Gottesman, Revisiting the role of ABC transporters in multidrug-resistant cancer, *Nat. Rev. Cancer*, 2018, **18**(7), 452–464.

7 Y. F. Fan, W. Zhang, L. Zeng, Z. N. Lei, C. Y. Cai, P. Gupta, *et al.*, Dacomitinib antagonizes multidrug resistance (MDR)

8 I. Genovese, A. Ilari, Y. G. Assaraf, F. Fazi and G. Colotti, Not only P-glycoprotein: amplification of the ABCB1-containing chromosome region 7q21 confers multidrug resistance upon cancer cells by coordinated overexpression of an assortment of resistance-related proteins, *Drug Resist. Updates*, 2017, **32**, 23–46.

9 W. K. Lee and F. Thevenod, Oncogenic PITX2 facilitates tumor cell drug resistance by inverse regulation of hOCT3/SLC22A3 and ABC drug transporters in colon and kidney cancers, *Cancer Lett.*, 2019, **449**, 237–251.

10 R. Hu, J. Gao, R. Rozimamat and H. A. Aisa, Jatrophane diterpenoids from *Euphorbia sororia* as potent modulators against P-glycoprotein-based multidrug resistance, *Eur. J. Med. Chem.*, 2018, **146**, 57–170.

11 S. Ding, N. Patel and H. J. Zhang, Ciclosporin A as a Reversal Agent Against Concurrent Multidrug Resistance in Tumors with Nanobubbles, *J. Biomed. Nanotechnol.*, 2018, **14**(1), 190–197.

12 K. Jin, S. Park, W. W. Teo, P. Korangath, S. S. Cho, T. Yoshida, *et al.*, HOXB7 Is an ERalpha Cofactor in the Activation of HER2 and Multiple ER Target Genes Leading to Endocrine Resistance, *Cancer Discovery*, 2015, **5**(9), 944–959.

13 P. Caetano-Pinto, J. Jansen, Y. G. Assaraf and R. Masereeuw, The importance of breast cancer resistance protein to the kidneys excretory function and chemotherapeutic resistance, *Drug Resist. Updates*, 2017, **30**, 15–27.

14 X. Ma, M. Hu, H. Wang and J. Li, Discovery of traditional Chinese medicine monomers and their synthetic intermediates, analogs or derivatives for battling P-gp-mediated multi-drug resistance, *Eur. J. Med. Chem.*, 2018, **159**, 381–392.

15 J. Yang, B. Zhang, Z. Qin, S. Li, J. Xu, Z. Yao, *et al.*, Efflux excretion of bisdemethoxycurcumin-*O*-glucuronide in UGT1A1-overexpressing HeLa cells: identification of breast cancer resistance protein (BCRP) and multidrug resistance-associated proteins 1 (MRP1) as the glucuronide transporters, *Biofactors*, 2018, **44**(6), 558–569.

16 Y. Xiao, L. Xin, L. Li, G. Li, X. Shi, G. Ji, *et al.*, Quercetin and kaempferol increase the intestinal absorption of isorhamnetin coexisting in *Elaeagnus rhamnoides* (L.) A. Nelson (Elaeagnaceae) extracts *via* regulating multidrug resistance-associated protein 2, *Phytomedicine*, 2019, **53**, 154–162.

17 B. Zhai, Y. Zeng, Z. Zeng, N. Zhang, C. Li, Y. Zeng, *et al.*, Drug delivery systems for elemene, its main active ingredient beta-elemene, and its derivatives in cancer therapy, *Int. J. Nanomed.*, 2018, **13**, 6279–6296.

18 Y. Zhang, J. P. Bressler, J. Neal, B. Lal, H. E. Bhang, J. Laterra, *et al.*, ABCG2/BCRP expression modulates D-luciferin based bioluminescence imaging, *Cancer Res.*, 2007, **67**(19), 9389–9397.

19 S. Lwano, M. Sugiyama, H. Hama, A. Watakabe, N. Hasegawa, T. Kuchimaru, *et al.*, Single-cell bioluminescence imaging of

deep tissue in freely moving animals, *Science*, 2018, **359**(6378), 935–939.

20 J. Li, L. Chen, L. Du and M. Li, Cage the firefly luciferin!- a strategy for developing bioluminescent probes, *Chem. Soc. Rev.*, 2013, **42**(2), 662–676.

21 R. Huang, J. Vider, I. Serganova and R. G. Blasberg, ATP-binding cassette transporters modulate both coelenterazine- and D-luciferin-based bioluminescence imaging, *Mol. Imaging*, 2011, **10**(3), 215–226.

22 K. Sasaki, M. Tachikawa, Y. Uchida, S. Hirano, F. Kadowaki, M. Watanabe, *et al.*, ATP-Binding Cassette Transporter A Subfamily 8 is a Sinusoidal Efflux Transporter for Cholesterol and Taurocholate in Mouse and Human Liver, *Mol. Pharm.*, 2018, **15**(2), 343–355.

23 Y. Zhang, M. Pullambhatla, J. Laterra and M. G. Pomper, Influence of Bioluminescence Imaging Dynamics by D-Luciferin Uptake and Efflux Mechanisms, *Mol. Imaging*, 2012, **11**(6), 499–506.

24 Y. Zhang, Y. Byun, Y. R. Ren, J. O. Liu, J. Laterra and M. G. Pomper, Identification of inhibitors of ABCG2 by a bioluminescence imaging-based high-throughput assay, *Cancer Res.*, 2009, **69**(14), 5867–5875.

25 A. Pichler, J. L. Prior and D. Piwnica-Worms, Imaging reversal of multidrug resistance in living mice with bioluminescence: MDR1 P-glycoprotein transports coelenterazine, *Proc. Natl. Acad. Sci. U. S. A.*, 2004, **101**(6), 1702–1707.

26 C. Y. Tang, L. X. Zhu, J. D. Yu, Z. Chen, M. C. Gu, C. F. Mu, *et al.*, Effect of beta-elemene on the kinetics of intracellular transport of D-luciferin potassium salt (ABC substrate) in doxorubicin-resistant breast cancer cells and the associated molecular mechanism, *Eur. J. Pharm. Sci.*, 2018, **120**, 20–29.

27 G. L. Beretta, G. Cassinelli, M. Pennati, V. Zuco and L. Gatti, Overcoming ABC transporter-mediated multidrug resistance: the dual role of tyrosine kinase inhibitors as multitargeting agents, *Eur. J. Med. Chem.*, 2017, **142**, 271–289.

28 V. GolerF-Baron and Y. G. Assaraf, Structure and function of ABCG2-rich extracellular vesicles mediating multidrug resistance, *PLoS One*, 2011, **6**(1), e16007.

29 Y. Miao, W. Zheng, N. Li, Z. Su, L. Zhao, H. Zhou, *et al.*, MicroRNA-130b targets PTEN to mediate drug resistance and proliferation of breast cancer cells *via* the PI3K/Akt signaling pathway, *Sci. Rep.*, 2017, **7**, 41942.

30 S. Mallappa, P. K. Neeli, S. Karnewar and S. Kotamraju, Doxorubicin induces prostate cancer drug resistance by upregulation of ABCG4 through GSH depletion and CREB activation: relevance of statins in chemosensitization, *Mol. Carcinog.*, 2019, e22996.

31 S. M. Stefan and M. Wiese, Small-molecule inhibitors of multidrug resistance-associated protein 1 and related processes: a historic approach and recent advances, *Med. Res. Rev.*, 2019, **39**(1), 176–264.

32 J. Zhang, Li Xiang and L. Huang, Non-viral nanocarriers for siRNA delivery in breast cancer, *J. Controlled Release*, 2014, **190**, 440–450.

33 Z. Chen, T. Shi, L. Zhang, P. Zhu, M. Deng, C. Huang, *et al.*, Mammalian drug efflux transporters of the ATP binding cassette (ABC) family in multidrug resistance: a review of the past decade, *Cancer Lett.*, 2016, **370**(1), 153–164.

34 A. Dlugosz and A. Janecka, ABC Transporters in the Development of Multidrug Resistance in Cancer Therapy, *Curr. Pharm. Des.*, 2016, **22**(30), 4705–4716.

35 M. Z. El-Readi, S. Eid, A. A. Abdelghany, H. S. Al-Amoudi, T. Efferth and M. Wink, Resveratrol mediated cancer cell apoptosis, and modulation of multidrug resistance proteins and metabolic enzymes, *Phytomedicine*, 2019, **55**, 269–281.

36 S. M. Thompson, M. R. Callstrom, B. E. Knudsen, J. L. Anderson, S. L. Sutor, K. A. Butters, *et al.*, Molecular bioluminescence imaging as a noninvasive tool for monitoring tumor growth and therapeutic response to MRI-guided laser ablation in a rat model of hepatocellular carcinoma, *Invest. Radiol.*, 2013, **48**(6), 413–421.

37 B. D. Furmanski, S. Hu, K. I. Fujita, L. Li, A. A. Gibson, L. J. Janke, *et al.*, Contribution of ABCC4-mediated gastric transport to the absorption and efficacy of dasatinib, *Clin. Cancer Res.*, 2013, **19**(16), 4359–4370.

38 J. Bakhsheshian, B. R. Wei, K. E. Chang, S. Shukla, S. V. Ambudkar, R. M. Simpson, *et al.*, Bioluminescent imaging of drug efflux at the blood-brain barrier mediated by the transporter ABCG2, *Proc. Natl. Acad. Sci. U. S. A.*, 2013, **110**(51), 20801–20806.